Materials Research Letters

ISSN: (Print) 2166-3831 (Online) Journal homepage: https://www.tandfonline.com/loi/tmrl20

Atom-probe study of Cu and NiAl nanoscale precipitation and interfacial segregation in a nanoparticle-strengthened steel

Z. B. Jiao, J. H. Luan, W. Guo, J. D. Poplawsky & C. T. Liu

To cite this article: Z. B. Jiao, J. H. Luan, W. Guo, J. D. Poplawsky & C. T. Liu (2017) Atom-probe study of Cu and NiAl nanoscale precipitation and interfacial segregation in a nanoparticle-strengthened steel, Materials Research Letters, 5:8, 562-568, DOI: 10.1080/21663831.2017.1364675

To link to this article: https://doi.org/10.1080/21663831.2017.1364675

Published online: 14 Aug 2017.

MATER. RES. LETT., 2017
VOL. 5, NO. 8, 562–568
https://doi.org/10.1080/21663831.2017.1364675

MATERIALS RESEARCH LETTERS
Taylor & Francis
Taylor & Francis Group

ORIGINAL REPORT

Atom-probe study of Cu and NiAl nanoscale precipitation and interfacial segregation in a nanoparticle-strengthened steel

Z. B. Jiao[a,b], J. H. Luan[a], W. Guo[c], J. D. Poplawsky[c] and C. T. Liu[a]

[a]Center for Advanced Structural Materials, Dept. of Mechanical and Biomedical Engineering, College of Science and Engineering, City University of Hong Kong, Hong Kong, People's Republic of China; [b]Dept. of Mechanical Engineering, The Hong Kong Polytechnic University, Hong Kong, People's Republic of China; [c]Center for Nanophase Materials Sciences, Oak Ridge National Laboratory, Oak Ridge, TN 37831, USA

ABSTRACT

The Cu and NiAl nanoscale precipitation and interfacial segregation in the martensite and austenite phases within a high-strength steel were studied by atom-probe tomography (APT). In the martensite phase, APT reveals the precipitation of isolated NiAl nanoparticles and NiAl/Cu co-precipitates, indicating that NiAl nanoparticles form first in the precipitation sequence. In comparison, the austenite phase contains only Cu nanoparticles with Ni segregation at the particle/matrix interface, in which the Ni segregation reduces the Cu nanoparticle interfacial energy. In addition, Mn and C exhibit an enrichment at the martensite/austenite interface, and the mechanism for the interfacial segregation was also discussed.

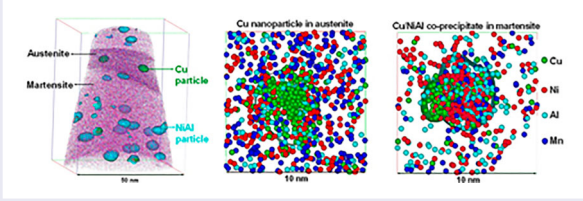

IMPACT STATEMENT

The understanding of nanoscale precipitation and interfacial segregation mechanism provides the basis for the control of precipitate microstructures and mechanical properties of nanoparticle-strengthened steels.

ARTICLE HISTORY
Received 11 May 2017

KEYWORDS
Cu and NiAl precipitate; nanoscale precipitation; interfacial segregation; high-strength steel; atom-probe tomography

Introduction

Precipitation of nanoparticles has been recognized as one of the most effective methods to increase the strength of steels, and precipitation hardening has become the foundation in the development of many grades of high-strength steels [1–8]. It is known that the degree of strengthening so obtained is highly dependent upon the precipitate microstructure, including the structure, morphology, size, and interparticle spacing of the nanoparticles [9]. Fundamentally, the precipitate microstructure is determined by the thermodynamic properties, such as the elastic and interfacial energies as well as the chemical driving force for precipitation, and the kinetics of the system, which, in turn, are strongly affected by the composition and crystal structure of the matrix [10]. In other words, the precipitation behavior of specific nanoparticles can be significantly different in different matrix phases. Practically, for many high-strength steels, the matrix is tailored to have a mixture of two or more phases, rather than simply a single phase, to obtain an optimum combination of high strength and high ductility [11–14]. Among them, Cu and NiAl nanoparticle-strengthened steels represent an important class of advanced high-strength steels, which have attracted significant attention in recent years due to their good combination of high strength, good ductility, and good weldability [15–22]. It was found that there are two types of pathways for the formation of the NiAl/Cu co-precipitates in the martensite phase (i.e. 'solid solution → Cu particles → Cu particles + NiAl particles' and 'solid solution → NiAl particles → NiAl particles + Cu particles'), depending upon the Cu, Ni, and Al concentrations [21,22]. In addition, the welding study revealed that the NiAl/Cu co-precipitates which are dissolved in the matrix during

CONTACT C. T. Liu chainliu@cityu.edu.hk

welding can be re-precipitated upon proper post-weld heat-treatments, leading to a recovery of the strength [22]. It should be pointed out that the matrix of most Cu and NiAl nanoparticle-strengthened steels is primarily martensite, but contains a small amount of austenite, the amount of which depends on the alloy composition and heat-treatment histories. While most of the previous studies were focused mainly on the understanding of precipitation behavior of Cu and NiAl nanoparticles in the martensite and ferrite phases [15–22], limited detailed information is available on the precipitation behavior and related mechanism in the austenite phase. Recently, in a welding study of a newly developed Cu/NiAl co-precipitation strengthened steel [22], we observed an interesting microstructure containing both martensite and austenite phases together with complex nanoscale precipitation behavior in the heat-affected zone. Although the thermal history of the heat-affected zone is complicated in nature, while for an understanding of the welding microstructure, it is interesting and important to study the precipitation behavior and interfacial segregation in the heat-affected zone. In this Letter, we intend to investigate this interesting microstructure in detail and comparatively study the precipitation and segregation behavior in the martensite, austenite, and their interfaces, aiming at elucidating the basic mechanism involved in the nanoscale precipitation, interfacial segregation, and solute partitioning in different matrix phases, which has not been well understood yet. The precipitation characteristics, including the size, morphology, and composition of Cu and NiAl nanoparticles in the alloy, were investigated by atom-probe tomography (APT). Particular attentions were paid to understanding the Cu and NiAl nanoscale precipitation in the martensite and austenite phases as well as the interfacial segregation behavior at the martensite/austenite interface.

Experimental

The chemical composition of the steel was Fe-5Ni-2Al-3Mn-1.5Cu-1.5Mo-1.5W-0.07Nb-0.05C-0.01B (wt.%). Alloy ingots were solution-treated at 900°C for 30 min, followed by water quenching and aging at 550°C for 2 h. The plates were welded using the arc welding technique [22], and needle-shaped specimens for APT studies were fabricated by lift-outs from the heat-affected zone and annular milled in a FEI Nova 200 focused ion beam/scanning electron microscope (FIB/SEM). The APT characterizations were performed in a local electrode atom probe (CAMEACA LEAP 4000X HR). The APT specimens were analyzed in voltage mode with a specimen temperature of 50 K, a pulse repetition rate of 200 kHz, a pulse fraction of 20%, and an evaporation detection rate of 0.5% atom per pulse. Imago Visualization and Analysis Software version 3.6.12 was used for the 3D reconstructions and data analysis.

Results and discussion

Atom maps of Ni (red), Mn (blue), Al (cyan), Cu (green), and C (wine) taken from the APT analysis of the steel are shown in Figure 1(a–e), respectively, and their overlay is displayed in Figure 1(f). The atom maps reveal a complex but interesting nanostructure containing three types of compositional features: (i) a Ni-, Mn-, Cu-, and C-enriched phase at the upper middle portion of the maps, (ii) the rest of the matrix enriched in Al and depleted in Ni, Mn, Cu, and C, and (iii) high number densities of spherical nanoparticles with sizes of 1–5 nm, most of which are enriched in Ni, Al, Cu, and Mn. It is well known that Ni, Mn, Cu and C are all austenite stabilizers and preferred to partition in the austenite phase, whereas Al, as a ferrite stabilizer, tends to concentrated in the ferrite/martensite phase [23]. In addition, the previous study revealed that the specimen contains martensite together with a small amount of austenite [22]. Therefore, it is reasonable to presume that the Ni/Mn/Cu/C-enriched phase is austenite, while the rest of the matrix enriched with Al is martensite.

To quantitatively measure the solute partitioning between the austenite and martensite phases and the solute segregation at the interphase boundary, a one-dimensional concentration profile was performed through the martensite/austenite interface shown in Figure 2(a). The region the concentration profile was taken has dimensions of 25 nm × 25 nm × 11 nm and is shown by yellow in Figure 1(f). The Ni, Mn, Cu, and C contents decrease from austenite to martensite, whereas the Al and Fe contents behave in an opposite way. In addition, Mn and C exhibit a strong segregation at the interface between the austenite and martensite phases, achieving peak concentrations of approximately 9 and 3 at.%, respectively. The composition of the austenite and martensite phases derived from the plateau data points on the concentration profiles are summarized in Figure 2(b). The concentrations of Ni, Mn, Cu, and C in the austenite phase ($\sim 6.6 \pm 0.4$, 7.3 ± 0.4, 1.8 ± 0.5, and 2.0 ± 0.1 at.%, respectively) are much higher than those in the martensite phase ($\sim 4.6 \pm 0.3$, 2.7 ± 0.2, 0.9 ± 0.1, and 0.2 ± 0.1 at.%, respectively). In contrast, the Al level in the austenite phase ($\sim 3.1 \pm 0.2$ at.%) is lower than that in the martensite phase ($\sim 3.7 \pm 0.3$ at.%).

Isoconcentration surfaces at 10 at.% Cu and 20 at.% (Ni + Al) were used to visualize and identify the Cu- and NiAl-enriched nanoparticles, respectively. The spatial distribution of the two types of nanoparticles, together

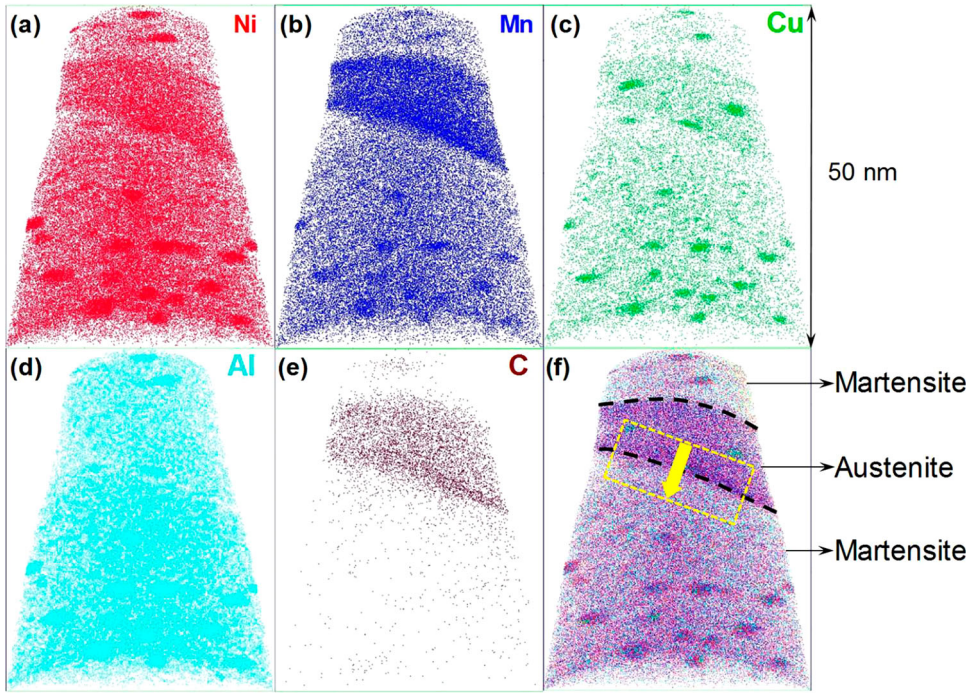

Figure 1. Atom maps of Ni, Mn, Cu, Al, and C in the Fe-Ni-Mn-Al-Cu-based steel.

with the solute atoms showing the location of the austenite and martensite phases, is displayed in Figure 3. In the austenite phase, only Cu nanoparticles were observed, and no NiAl nanoparticles were detected. The average radius of the Cu nanoparticles is estimated to be $\sim 2.0 \pm 0.1$ nm. In comparison, high number densities of both Cu and NiAl nanoparticles can be observed in the martensite phase. A statistical analysis of the particle configuration reveals that the majority ($77 \pm 5\%$) of the NiAl nanoparticles are NiAl/Cu co-precipitates, in which Cu nanoparticles are located on the outside surface of NiAl particles, and only a small fraction ($23 \pm 5\%$) of NiAl nanoparticles are isolated particles without any Cu particles associated with them. It is worthwhile to point out that no isolated Cu nanoparticles were detected in the martensite phase. The average radius of the Cu nanoparticles in the martensite phase was determined to be $\sim 1.1 \pm 0.3$ nm, smaller than that in the austenite phase ($\sim 2.0 \pm 0.1$ nm), whereas that of the NiAl nanoparticles was found to be $\sim 1.8 \pm 0.9$ nm.

To understand the partitioning behavior of solute atoms in the Cu and NiAl nanoparticles, 1-nm-thick atom maps through the centers of a Cu nanoparticles in the austenite phase, a NiAl/Cu co-precipitate in the martensite phase, and an isolated NiAl nanoparticle in the martensite phase are shown in Figure 4(a–c), respectively, in which the relative positions and extents of the Ni (red), Mn (blue), Cu (green), and Al (cyan) atoms are also indicated. The Cu nanoparticle in the austenite phase (Figure 4(a)) is embedded in a Ni- and Mn-enriched austenite phase. The center of the Cu particle is almost free of Ni and Mn, whereas a considerable amount of Ni and Mn can be observed at the Cu particle/austenite interface. In comparison, a Cu particle is located on the outside surface of a NiAl particle in the martensite phase (Figure 4(b)), and the two particles overlap largely with each other. For the isolated NiAl nanoparticle in martensite (Figure 4(c)), Ni and Al together with a small amount of Mn and Cu are partitioned to the particles, and there is no solute segregation at the NiAl particle/matrix interface. The quantification of the solute partitioning between the nanoparticles and matrix was determined from proximity histograms. The proximity histograms of the Cu nanoparticles in the austenite phase, and Cu and NiAl nanoparticles in the martensite phase are displayed in Figure 4(d–f), respectively, and the quantitative composition analysis of the nanoparticles is summarized in Figure 4(g). For the Cu particles in austenite (Figure 4(d)), the partitioning of Cu and Al to the particles and the partitioning of Fe and Mn to the matrix is clearly evident, whereas Ni exhibits a local segregation (~ 10 at.%) at the Cu particle/matrix interface and a strong depletion in the Cu nanoparticles. The Cu nanoparticles consist mainly of Cu ($\sim 88.5 \pm 6.3$ at.%) together with a small amount of Fe ($\sim 7.7 \pm 5.2$ at.%) and Al ($\sim 3.9 \pm 3.7$ at.%). The Cu particles in martensite are enriched in Cu ($\sim 44.6 \pm 5.8$ at.%) but contain a significant amount of Ni ($\sim 12.2 \pm 3.8$ at.%), Al ($\sim 20.3 \pm 4.7$ at.%), Mn

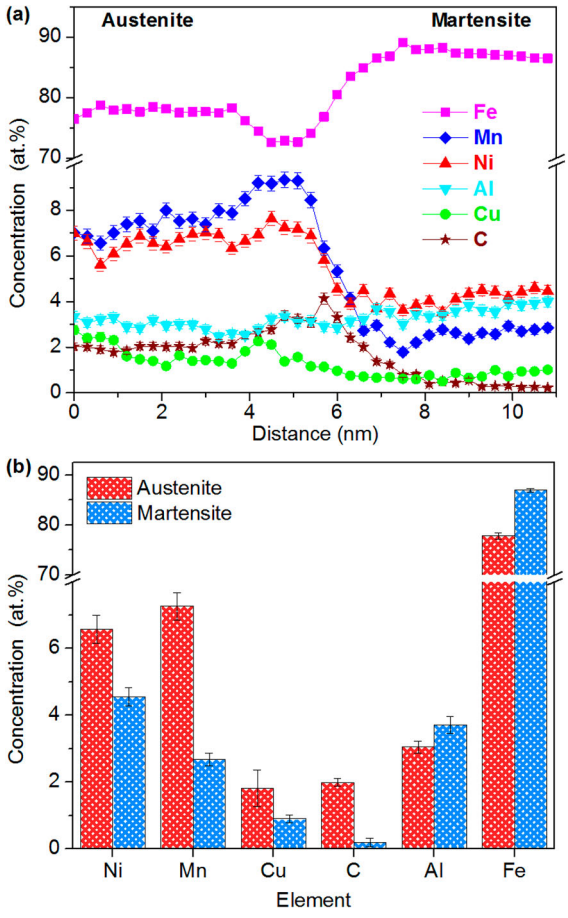

Figure 2. (a) Concentration profile across an austenite-martensite interface and (b) compositions of the austenite and martensite phases.

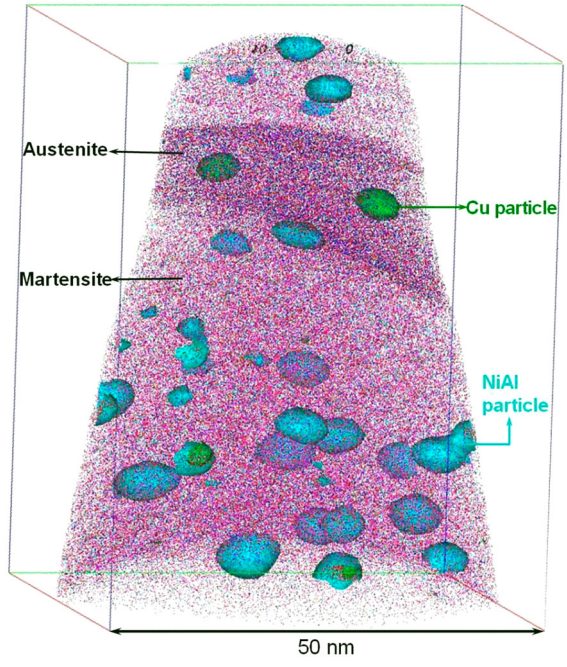

Figure 3. Cu and NiAl nanoparticles together with solute atom maps showing the austenite and martensite phases in a 3D reconstruction.

(~9.5 ± 3.4 at.%), and Fe (~13.5 ± 4.0 at.%), indicating that the composition of the Cu particles in martensite is far from equilibrium. In addition, a pronounced segregation of Ni, Al, and Mn at the Cu particle/martensite interface can be observed, consistent with previous studies on Cu and NiAl nanoparticle-strengthened martensitic steels [15–22]. For the NiAl particles in martensite (Figure 4(f)), the enrichment of not only Ni and Al, but also Mn and Cu change monotonically toward the center of the NiAl nanoparticles, and the concentration of Ni, Al, Mn, Cu, and Fe of the particles are estimated to be 39.1 ± 2.3, 26.8 ± 2.1, 9.7 ± 1.4, 15.4 ± 1.7, and 8.6 ± 1.3 at %, respectively.

The APT results presented above indicate that the Cu and NiAl nanoparticles exhibit different precipitation behavior in the martensite and austenite phases together with interesting solute segregation at the martensite/austenite interface. For an understanding to eventually control the complex precipitation and segregation behavior, it is of fundamental importance to elucidate the basic mechanism involved in the precipitation of Cu and NiAl nanoparticles in the martensite and austenite phases as well as the interfacial segregation at the interface between the two phases.

First, the co-precipitation mechanism of Cu and NiAl nanoparticles in martensite will be briefly summarized for a comparison with that in austenite. It has been generally recognized that there are two types of precipitation pathways for the formation of the NiAl/Cu co-precipitates, depending mainly upon the Cu/Ni and Cu/Al ratios [24]. In the current steel, NiAl nanoparticles, enriched in Ni, Al and Cu, nucleate first from the supersaturated solid solution, and Cu solutes are rejected to the NiAl particle surface at later stages of precipitation, leading to the precipitation of Cu nanoparticles on the outer surface of NiAl nanoparticles [22].

Second, the precipitation mechanism in the austenite phase will be discussed. APT reveals the precipitation of 4-nm-diameter Cu nanoparticles in the austenite phase. From the nucleation point of view, the interfacial energy and strain energy play an important role in the formation of nanoparticles in a supersaturated solid solution [10]. The lattice constants of fcc-Cu and fcc-Fe are 3.61 and 3.65 nm [25], respectively. The very small difference between their lattice constant leads to a very small strain energy and, hence, favors a coherent interface between the fcc Cu nanoparticles and austenite matrix. Therefore, the Cu nanoparticles in the fcc austenite phase are expected to directly form with a fcc equilibrium structure of Cu, the formation of which is different from the initial structure of bcc Cu nanoparticles in the bcc ferrite/martensite phase [26,27]. In addition, the segregation of Ni has been observed at the interface between

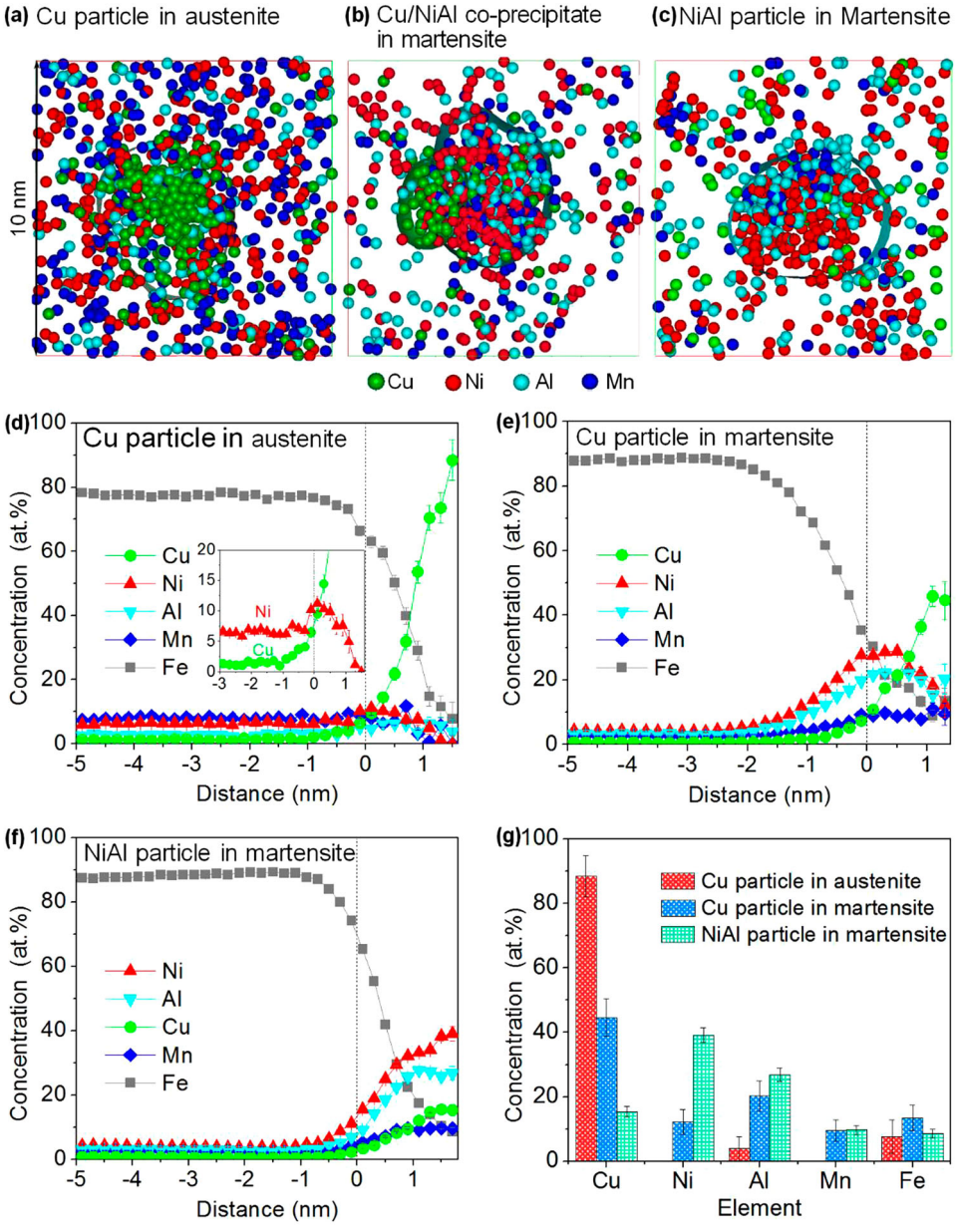

Figure 4. 1-nm-thick atom maps of (a) a Cu nanoparticle in austenite, (b) a NiAl/Cu co-precipitate in martensite, and (c) an isolated NiAl nanoparticle in martensite, proximity histograms of (d) Cu nanoparticles in austenite and (e) Cu and (f) NiAl nanoparticles in martensite, and (g) compositions of the three types of nanoparticles.

the Cu nanoparticles and the austenite matrix, which is similar to but less pronounced than that as observed for the Cu precipitation in ferrite/martensite [15–22]. It is known that the heat of mixing between Fe and Cu is large and positive (+13 kJ mol^{-1}), whereas that for both Fe–Ni and Cu–Ni pairs is very small (−4 and +2 kJ mol^{-1}, respectively) [28]. As a result, the interfacial segregation of Ni can act as a buffer layer to further reduce the interfacial free energy between the Cu-enriched nanoparticles and the Fe-enriched matrix, thereby promoting the precipitation of Cu nanoparticles. Furthermore, it is worthy to point out that the austenite phase containing Cu nanoparticles in the as-welded condition is probably in a non-equilibrium state due to the complicated thermal history of welding. After a post-weld heat-treatment for 30 min at 550°C, the microstructure is much more close to an equilibrium state, and no Cu particles can be observed in the austenite phase [22]. Lastly, it is interesting to note that, unlike that in martensite, no NiAl nanoparticles were formed in austenite. The reasons for the absence of NiAl nanoparticles could be twofold. One is the depletion of Al in the austenite phase (Figure 2), as Al is known as a ferrite stabilizer and tends to partition to ferrite/martensite and deplete in austenite; the other

reason is the relative higher solubility of Ni in austenite (fully miscible) as compared with that in martensite (< 5.5 at.%) [23]. Both result in a low chemical driving force for the precipitation of NiAl nanoparticles in the austenite phase.

Third, the solute segregation at the martensite/austenite interface will be analyzed. As illustrated in Figure 2(a), carbon shows a very sharp segregation peak at the martensite/austenite interface, whereas the Mn segregation extends widely up to almost 2 nm and shifts to the left side (the austenite phase). The reason for the relatively wide Mn segregation is probably that the partitioning of Mn results from a lower diffusion coefficient of Mn in austenite than in martensite, and upon heat treatment the flux of Mn cannot be quickly accommodated and thus partitions in the austenite adjacent to the martensite/austenite interface. It is generally observed that Mn partitions in the Mn-stabilizer phase, where the diffusivity of Mn is lower than its neighboring phase [11,29]. For carbon, there is no such kinetic problem, and thus, a partitioning of carbon is not expected and not observed in Figure 2(a). Therefore, it can be speculated that the C segregation peak marks the position of the martensite/austenite interface, and the extended segregation zone of Mn should be austenite. In addition, as mentioned above, the austenite phase in the as-welded condition is probably in a non-equilibrium state. After a post-weld heat-treatment for 30 min at 550°C, the partitioning of Mn between the martensite and austenite phases is more close to an equilibrium state, and both C and Mn show the segregation at the martensite/austenite interface [22].

Conclusions

In summary, the precipitation behavior of Cu and NiAl nanoparticles in the martensite and austenite phases and the interfacial segregation between the two phases have been studied by APT. In the martensite phase, APT reveals the precipitation of NiAl/Cu co-precipitates and isolated NiAl nanoparticles, but no isolated Cu nanoparticles, which supports the precipitation mechanism that NiAl nanoparticles form earlier than Cu nanoparticles in the precipitation sequence. In comparison, the austenite phase shows only Cu nanoparticles with Ni segregation at the particle/matrix interface, which favors the reduction of interfacial energies for Cu nanoparticles. Due to the lattice coherency, the Cu nanoparticles in the fcc austenite phase are expected to directly form with the fcc structure, rather than the bcc Cu nanoparticles formed in the bcc ferrite/martensite phase. The absence of NiAl nanoparticles in the austenite phase is due to the depletion of Al and the large solubility of Ni in austenite, both resulting in a low chemical driving force for NiAl precipitation. In addition, carbon shows a very sharp segregation peak at the martensite/austenite interface, whereas Mn segregation extends widely up to almost 2 nm and shifts to the austenite side due to its lower diffusivity in austenite as compared with that in martensite. This knowledge would be helpful in understanding and control of the precipitation behavior of high-strength steels.

Acknowledgement

Atom-probe tomography was conducted at ORNL's Center for Nanophase Materials Sciences (CNMS), which is a U.S. DOE Office of Science User Facility.

Disclosure statement

No potential conflict of interest was reported by the authors.

Funding

This research was supported by a grant from City University of Hong Kong (Project No.7004686), the General Research Fund (account No. CityU11205515) and the Collaborative Research Fund (account No. C1027-14E) supported by the Research Grant Council, Hong Kong.

References

[1] Sun Z, Song G, Ilavsky J, et al. Duplex precipitates and their effects on the room-temperature fracture behaviour of a NiAl-strengthened ferritic alloy. Mater Res Lett. 2015;3(3):128–134.
[2] Yen HW, Huang CY, Yang JR. Characterization of interphase-precipitated nanometer-sized carbides in a Ti–Mo-bearing steel. Scr Mater. 2009;61(6):616–619.
[3] Trotter G, Baker I. The effect of aging on the microstructure and mechanical behavior of the alumina-forming austenitic stainless steel Fe–20Cr–30Ni–2Nb–5Al. Mater Sci Eng A. 2015;627:270–276.
[4] Dou Y, Liu Y, Liu F, et al. Microstructures and mechanical properties of a Cu-bearing ODS steel fabricated by mechanical alloying and hot extrusion. J Nucl Mater. 2013;434:129–132.
[5] Wen YR, Hirata A, Zhang ZW, et al. Microstructure characterization of Cu-rich nanoprecipitates in a Fe–2.5Cu–1.5Mn–4.0Ni–1.0Al multicomponent ferritic alloy. Acta Mater. 2013;61:2133–2147.
[6] Millán J, Sandlöbes S, Al-Zubi A, et al. Designing Heusler nanoprecipitates by elastic misfit stabilization in Fe–Mn maraging steels. Acta Mater. 2014;76:94–105.
[7] Ping DH, Ohnuma M, Hirakawa Y, et al. Microstructural evolution in 13Cr–8Ni–2.5 Mo–2Al martensitic precipitation-hardened stainless steel. Mater Sci Eng A. 2005;394:285–295.
[8] Isheim D, Vaynman S, Fine ME, et al. Copper-precipitation hardening in a non-ferromagnetic face-centered cubic austenitic steel. Scr Mater. 2008;59:1235–1238.

[9] Ardell AJ. Precipitation hardening. Metall Trans A. 1985;16:2131–2165.
[10] Doi M. Elasticity effects on the microstructure of alloys containing coherent precipitates. Prog Mater Sci. 1996;40:79–180.
[11] Dmitrieva O, Ponge D, Inden G, et al. Chemical gradients across phase boundaries between martensite and austenite in steel studied by atom probe tomography and simulation. Acta Mater. 2011;59:364–374.
[12] Wang J, Wang Z, Wang X, et al. Strengthening effect of nanoscale precipitation and transformation induced plasticity in a hot rolled copper-containing ferrite-based lightweight steel. Scr Mater. 2017;129:25–29.
[13] He BB, Huang MX, Liang ZY, et al. Nanoindentation investigation on the mechanical stability of individual austenite grains in a medium-Mn transformation-induced plasticity steel. Scr Mater. 2013;69:215–218.
[14] Caballero FG, Miller MK, Clarke AJ, et al. Examination of carbon partitioning into austenite during tempering of bainite. Scr Mater. 2010;63:442–445.
[15] Kolli RP, Seidman DN. The temporal evolution of the decomposition of a concentrated multicomponent Fe–Cu-based steel. Acta Mater. 2008;56:2073–2088.
[16] Kapoor M, Isheim D, Ghosh G, et al. Aging characteristics and mechanical properties of 1600MPa body-centered cubic Cu and B2-NiAl precipitation-strengthened ferritic steel. Acta Mater. 2014;73:56–74.
[17] Kapoor M, Isheim D, Vaynman S, et al. Effects of increased alloying element content on NiAl-type precipitate formation, loading rate sensitivity, and ductility of Cu- and NiAl-precipitation-strengthened ferritic steels. Acta Mater. 2016;104:166–171.
[18] Vaynman S, Isheim D, Kolli RP, et al. High-strength low-carbon ferritic steel containing Cu-Fe-Ni-Al-Mn precipitates. Metall Mater Trans A. 2008;39:363–373.
[19] Schnitzer R, Schober M, Zinner S, et al. Effect of Cu on the evolution of precipitation in an Fe–Cr–Ni–Al–Ti maraging steel. Acta Mater. 2010;58:3733–3741.
[20] Jiao ZB, Luan JH, Miller MK, et al. Precipitation mechanism and mechanical properties of an ultra-high strength steel hardened by nanoscale NiAl and Cu particles. Acta Mater. 2015;97:58–67.
[21] Jiao ZB, Luan JH, Miller MK, et al. Group precipitation and age hardening of nanostructured Fe-based alloys with ultra-high strengths. Sci Rep. 2016;6:21364.
[22] Jiao ZB, Luan JH, Guo W, et al. Effects of welding and post-weld heat treatments on nanoscale precipitation and mechanical properties of an ultra-high strength steel hardened by NiAl and Cu nanoparticles. Acta Mater. 2016;120:216–227.
[23] Cahn RW, Haasen P. Physical metallurgy. 4th ed. Amsterdam: North-Holland; 1996.
[24] Jiao ZB, Luan JH, Miller MK, et al. Co-precipitation of nanoscale particles in steels with ultra-high strength for a new era. Mater Today. 2017;20(3):142–154. doi:10.1016/j.mattod.2016.07.002
[25] Ohresser P, Shen J, Barthel J, et al. Growth, structure, and magnetism of fcc Fe ultrathin films on Cu (111) by pulsed laser deposition. Phys Rev B. 1999;59:3696–3706.
[26] Goodman SR, Brenner SS, Low JR. An FIM-atom probe study of the precipitation of copper from lron-1.4 at. pct copper. Part II: atom probe analyses. Metall Trans. 1973;4:2363–2369.
[27] Othen PJ, Jenkins ML, Smith GDW, et al. Transmission electron microscope investigations of the structure of copper precipitates in thermally-aged Fe–Cu and Fe–Cu–Ni. Philo Mag Lett. 1991;64:383–391.
[28] Takeuchi A, Inoue A. Classification of bulk metallic glasses by atomic size difference, heat of mixing and period of constituent elements and its application to characterization of the main alloying element. Mater Trans. 2005;46:2817–2829.
[29] Li YJ, Kostka A, Choi P, et al. Mechanisms of subgrain coarsening and its effect on the mechanical properties of carbon-supersaturated nanocrystalline hypereutectoid steel. Acta Mater. 2015;84:110–123.